Catalysis Science & Technology

ROYAL SOCIETY OF CHEMISTRY

PAPER

View Article Online
View Journal | View Issue

Check for updates

Cite this: *Catal. Sci. Technol.*, 2021, 11, 5484

Selective oxidation of methane to methanol on dispersed copper on alumina from readily available copper(II) formate†

Jordan Meyet,[a] Alexander P. van Bavel,[b] Andrew D. Horton,[b] Jeroen A. van Bokhoven *[ac] and Christophe Copéret *[a]

Received 4th May 2021,
Accepted 8th July 2021

DOI: 10.1039/d1cy00789k

rsc.li/catalysis

The direct conversion of methane to methanol attracts increasing interest due to the availability of low-cost methane from natural gas. Significant steps in that direction have already been achieved, using a stepwise chemical looping approach employing zeolites, but these materials have limited industrial relevance, because of low methanol productivity and relatively high materials cost. We therefore investigated the reactivity of copper supported on γ-Al_2O_3 prepared by common synthetic routes, namely incipient wetness impregnation and specific adsorption. All materials showed reactivity for the partial oxidation of methane under mild conditions (6 bar, 200 °C), with increasing reactivity as the copper loading increases, leading to a maximum methanol yield of 15 μmol CH_3OH g^{-1}. A combination of spectroscopic techniques (UV-vis, XAS, EPR, TPR) allowed the assignment of the reactive species at low loading to the previously reported monomeric $[CuO(OH)]^-$ sites. This straightforward synthetic approach and spectroscopic characterization of the Cu(II) speciation can be applied to a wide range of oxide supports.

Open Access Article. Published on 08 July 2021. Downloaded on 5/21/2026 12:12:38 PM.
This article is licensed under a Creative Commons Attribution 3.0 Unported Licence.

Introduction

The increasing amount of methane available at low-cost from natural gas and oil field extraction, combined with the lack of efficient small-scale processes for its valorisation, has led to its flaring at remote extraction locations. Research towards the direct conversion of methane to value-added products has thus been an active field of research in the past decades, with specific interest in its direct transformation to methanol.[1–4] Methanol is particularly attractive because it can be used as an alternative energy carrier or further upgraded into higher-value chemicals. One of the challenges for this direct transformation concerns the selectivity towards the desired methanol at higher conversion, because the latter is more reactive than methane and its conversion to over-oxidized products (CO_2, CO) is thermodynamically favored. To address this problem, strategies to protect the desired product have been developed. For example, the further oxidation of methanol can be prevented through the formation of methyl bisulfate in the case of the catalytic (homogeneous) Periana system[5] and through the formation of surface methoxy intermediates in heterogeneous systems *via* chemical looping (cyclic process) that allows the decoupling of the methane oxidation steps and the formation of methanol.[6,7] In Nature, methane monooxygenases (MMO), which exist in two forms, soluble (sMMO) and particulate (pMMO), can perform this challenging transformation under aerobic condition with iron- and copper-containing active sites, respectively.[8] Inspired by this system, transition-metal exchanged zeolites have been developed and show promising results for this direct transformation.[9–11] Several limitations exist for their potential integration into a commercially relevant process. In the case of Fe-containing zeolites, the necessity of using N_2O as oxidant has been an obstacle for further research due to the high price of this oxidant compared to the targeted product.[12] In contrast, Cu-based materials use O_2, a cheap and readily available oxidant. Despite great improvements toward more efficient materials in the past decade,[9,10] economic studies on the feasibility of a cyclic process employing Cu-exchanged zeolites conclude that the implementation of these materials faces severe limitations: low methanol productivity due to the low content of active sites and long cycling times, in addition to the relatively high cost of the crystalline aluminosilicate framework. This has led to the investigation of other supports, such as silica[13,14] and alumina.[15] With silica as a support material, the observed reactivity towards methane was attributed to small CuO

[a] *Department of Chemistry and Applied Biosciences, ETH Zurich, Vladimir-Prelog-Weg 1-5, 8093 Zürich, Switzerland. E-mail: jeroen.vanbokhoven@chem.ethz.ch, ccoperet@inorg.chem.ethz.ch*
[b] *Shell Global Solutions International B.V, Grasweg 31, 1031 HW Amsterdam, The Netherlands*
[c] *Laboratory for Catalysis and Sustainable Chemistry, Paul Scherrer Institute, Villigen 5232, Switzerland*

† Electronic supplementary information (ESI) available. See DOI: 10.1039/d1cy00789k

This journal is © The Royal Society of Chemistry 2021

Open Access Article. Published on 08 July 2021. Downloaded on 5/21/2026 12:12:38 PM.
This article is licensed under a Creative Commons Attribution 3.0 Unported Licence.

particles, limiting the site density efficiency of such materials.[13] In comparison, using alumina as support produced well-dispersed copper sites that are active for the selective conversion of methane to methanol. However, the formation of the Cu(II) sites was based on rather elaborate synthetic approaches, using complex molecular precursors and leading to a mixed Al/Si environment.[15] Recent work in our laboratory revealed the presence of the same active monomeric site on a broad range of transition aluminas (γ-, η-, θ-), when generating the Cu centre in a pure Al environment, with a loading limited to 0.5 wt% Cu inherent to the complex preparation method relying on surface organometallic chemistry (SOMC) approach.[16]

This conclusion led us to explore the possibility of increasing the density of copper sites, while maintaining dispersion and monomeric active sites by using alternative simpler and cheaper synthesis protocols.

We explored incipient wetness impregnation (IWI) and specific adsorption (SA) as synthetic methods to vary the copper site density, to determine whether they would lead to similar intrinsic reactivity with increasing the copper loading on alumina while retaining the dispersion of the active centre. Towards this goal, we used a readily available monomeric copper molecular precursor for both methods, namely $[Cu(\kappa^2\text{-}OCHO)_2(tmeda)]$.[17] This specific compound was selected because it is monomeric, soluble both in organic and aqueous solvents and easy to synthesize on a large scale from commercially available reagents, copper(II) formate and tetramethyl ethylenediamine (tmeda). All synthesized materials, irrespective of the employed synthesis method, demonstrated good reactivity with methane under mild conditions (200 °C), leading to the formation of methoxy surface intermediates. At low copper loadings, the reactive site was assigned to the previously reported monomeric Cu(II) present on the (110) facet of alumina.[16] At higher loadings (3.2 wt% Cu; 1.3 Cu nm^{-1}), in addition to the monomeric species, other active species, possibly small copper oxide (CuO) clusters, are also present.

Experimental section

Synthetic procedure

General consideration. γ-Alumina (γ-Al_2O_3, Sasol Puralox® sBa 200) was compacted by combining with MilliQ water, drying at 100 °C for 24 h, and sieving to retain 250–450 μm aggregates. Copper formate (97%) and *N*,*N*,*N*′,*N*′-tetramethylenediamine (99%) were purchased from Sigma-Aldrich and used without further purification. Mili-Q water was purified using a Synergy® UV water purification system (18 MΩ cm). Acetonitrile was purchased from VWR and used as received. $[Cu(\kappa^2\text{-}OCHO)_2(tmeda)]$ (**1**) was prepared following a reported procedure.[17] The synthetic air for the activation was purified over activated molecular sieves (MS 4A).

Preparation of IWI samples. The sieved γ-Al_2O_3 was calcined under static air for 4 h at 500 °C (5 °C min^{-1}), dehydroxylated under high vacuum (10^{-5} mbar) for an additional 15 h ($Al_2O_{3\text{-}500}$) and stored in a glovebox under inert condition in between the different material preparations. The specific surface area and pore volume of Al_2O_3 was determined by N_2 adsorption (S_{BET} = 230 m^2 g^{-1}, V_p = 0.54 mL g^{-1}). The pore volume was also determined experimentally and is similar to the value obtained by N_2 adsorption (0.6 mL g^{-1}). Typical syntheses were performed on approximately 2.0 g of $Al_2O_{3\text{-}500}$ contacted with 0.6 mL g^{-1} of a solution containing **1** in water. The concentration of the solution was determined based on the targeted loading, with 0.13, 0.27, 0.53 and 1.06 mmol mL^{-1} to achieve 0.5, 1.0, 2.0, and 4.0 wt% Cu respectively. The solution was added dropwise in portions and stirred manually between each addition. After completion of the impregnation, the samples were dried at room temperature for 1 day and then placed in a U-tube flow reactor and thermally treated under flow of dry synthetic air (40 mL min^{-1}) at 80 °C (1 °C min^{-1}) for 2 h, 100 °C (1 °C min^{-1}) for 2 h, followed by calcination at 500 °C (5 °C min^{-1}) for 2.5 h. The reactor was evacuated at room temperature and the material was stored in a glovebox under inert atmosphere. Two different sets of materials were obtained employing this method.

$Cu_{IWI\text{-}0.3}$: EA_1: 0.33 wt% Cu, EA_2: 0.33 wt% Cu; **$Cu_{IWI\text{-}1}$**: EA_1: 0.96 wt% Cu, EA_2: 0.75 wt% Cu; **$Cu_{IWI\text{-}1.6}$**: EA_1: 1.64 wt% Cu, EA_2: 1.68 wt% Cu; **$Cu_{IWI\text{-}3.2}$**: EA_1: 3.19 wt% Cu, EA_2: 2.89 wt% Cu.

Preparation of SA samples. Approximately 1.0 g of $Al_2O_{3\text{-}500}$ was contacted with *ca.* 5 mL of solution of **1** in acetonitrile. The amount of **1** was determined based on the targeted loading, with 0.082 mmol, 0.17, 0.37 and 0.69 mmol of **1** used to achieve a maximum loading of 0.5, 1.0, 2.0, and 4.0 wt% Cu respectively. The solution was added at once to $Al_2O_{3\text{-}500}$ and stirred mechanically for 3 h before removing the supernatant and washing the material three times with diethyl ether, to remove any non-adsorbed molecular complex. The samples were dried under vacuum for 1 h before being placed in a U-tube flow reactor and thermally treated under flow of dry synthetic air (40 mL min^{-1}) at 100 °C (1 °C min^{-1}) for 2 h, followed by calcination at 500 °C (5 °C min^{-1}) for 2 h. The reactor was evacuated at room temperature and the material was stored in a glovebox under inert atmosphere.

$Cu_{SA\text{-}0.5}$: EA: 0.57 wt% Cu; **$Cu_{SA\text{-}1}$**: EA: 1.11 wt% Cu; **$Cu_{SA\text{-}1.5}$**: EA: 1.54 wt% Cu; **$Cu_{SA\text{-}1.8}$**: EA: 1.78 wt% Cu.

Reactivity study. Around 0.5 g of the calcined material was placed in a glass Fisher–Porter reactor (140 mL volume) under inert conditions, evacuated and filled with 3.7 bar of CH_4 at room temperature. The closed reactor was then heated to 200 °C in a tubular oven (5 °C min^{-1}), leading to an increase in pressure to 6 bar. The reactor temperature was maintained for 30 min. After removal of excess CH_4 under a flow of argon, the reactor was cooled down to room temperature under an argon flow, introduced inside a glovebox under inert conditions. The material was then placed in a double Rotaflo® under inert conditions and treated with approximately 1.5 mL of degassed water. After degassing the solution by freeze–pump–thaw, the mixture

Open Access Article. Published on 08 July 2021. Downloaded on 5/21/2026 12:12:38 PM.
This article is licensed under a Creative Commons Attribution 3.0 Unported Licence.

was then boiled in the closed vessel at 120 °C for 30 min. The aqueous phase containing the extracted CH_3OH was then isolated by vacuum distillation at liquid nitrogen temperature, followed by filtration through a 0.25 μm HPLC filter and analysed by GC.

Physicochemical characterization

Elemental analysis. The metal content was determined by inductively coupled plasma optical emission spectroscopy (ICP-OES). The ICP-OES was conducted at Mikroanalytisches Labor Pascher located in Remagen, Germany.

N_2 adsorption. Nitrogen adsorption isotherms at −196 °C were recorded on a Bel-Mini apparatus (Bel-Japan). The material was introduced in the glass tube under inert atmosphere and recorded without further outgassing. The BET method was applied to calculate the total surface area.

Infrared spectroscopy. Diffuse reflectance infrared Fourier transform (DRIFT) spectra were recorded without further dilution under inert atmosphere in a glovebox using a Bruker Alpha FT-IR spectrometer with 32 scans and 2 cm^{-1} resolution.

UV-vis spectroscopy. Diffuse reflectance UV-vis (DRUV-vis) spectra were recorded at room temperature on an Agilent Cary 5000 UV-vis-NIR spectrometer equipped with a Harrick Scientific Praying Mantis™ diffuse reflectance accessory (200–1200 nm). The sample was grinded into a fine powder and placed in an ambient sample chamber inside a glovebox and isolated under inert atmosphere. The spectra were recorded in absolute reflectance (R_∞) with a scanning rate of 600 nm min^{-1} and a spectral resolution of 1 nm. The Kubelka–Munk ($F(R_\infty)$) was calculated using the following formula: $F(R_\infty) = (1 - R_\infty)^2/(2 \times R_\infty)$.

Electron paramagnetic resonance (EPR) spectroscopy. The EPR spectra of the supported materials were recorded at room temperature on a Magnettech MS-5000 (Freiberg Instruments) at 6 mW in a quartz EPR tube equipped with a J Young valve, loaded under inert atmosphere. For the *in situ* reaction with CH_4, a high-pressure quartz EPR tube was loaded with the solid material, then spectra were recorded before and after introduction of CH_4 to ensure that no spectroscopic changes occurred. After loading the EPR tube with 3.7 bar of CH_4 at room temperature, the sample was warmed in the spectrometer at 200 °C (6 bar of CH_4) for 30 min. After reaction, the EPR spectrum was recorded again at room temperature. The data processing of the spectra was performed using ESR studio. The error for the double integral spin quantification was determined by performing the reaction *in situ* under argon atmosphere with $\mathbf{Cu_{IWI\text{-}1.6}}$ and was found to be 3% (error bars on Fig. S12†).

Temperature programmed reduction (TPR). TPR experiments were carried out using a BELCAT-B apparatus (Bel-Japan) using a cell equipped with a bypass, allowing the transfer of the sample from a glovebox to the instrument under inert conditions. The dried sample (200 mg) was introduced into the cell inside a glovebox and isolated before bringing out of the glovebox. The bypass was purged with argon for 30 min prior to contacting the sample with the gas inlet. The measurement was performed from 20 to 800 °C in a gas flow consisting of H_2/Ar (5 : 1, 30 ccm) using a ramp of 10 °C min^{-1}. The gas released was analysed using a calibrated TCD detector and a mass- spectrometer (Bel-Mass).

Powder X-ray diffraction (pXRD). pXRD patterns were recorded in reflection on a PANalytical X'Pert PRO-MPD diffractometer at a voltage of 30 kV and a current of 10 mA by applying Cu-Kα radiation (λ = 1.54060 Å). The data were recorded between 5 and 70° with 1/4° step for a duration of 1.5 s per step and plotted with correction of the background.

For the SA sample, powder XRD were recorded in transmission on a Stoe STADIP Dual Setup with a Mythen detectors at a voltage of 40 kV and a current of 35 mA by applying Cu-Kα radiation (λ = 1.54060 Å). The data were recorded between 3 and 85° with 0.2° step for a duration of 3 s per step and plotted without background correction.

X-ray adsorption spectroscopy. XAS measurements were carried out at the XAFS beamlines[18] of Elettra Sincrotrone Trieste, Italy. Cu K-edge XAS was collected in transmission, using a double crystal Si (111) monochromator and ionization chambers for normalization of the beam and energy calibration (Cu foil). The beam dimension used was 1.3 mm (v) × 1.5 mm (H), and the spectra where average over 8 scans. The calibration of the monochromator energy position was performed on a Cu foil spectrum (8979 eV) recorded simultaneously with the sample. The samples were pressed in pellets (7 mm diameter) with optimized thickness for transmission detection and placed in aluminized plastic bags (polyaniline (14 μm), polyethylene (15 μm), Al (12 μm), polyethylene (75 μm)) from Gruber-Folien GmbH & Co. KG using an impulse sealer inside an argon filled glovebox to avoid air contamination.

Gas chromatography (GC) analysis. The extracted CH_3OH in water was analysed using an aqueous isopropanol solution (10 mM) as internal standard (4 : 1 v : v) using GC/FID (Agilent Technologies 7890A) equipped with a splitless injector heated to 160 °C, injection volume 0.3 μl using hydrogen carrier gas. Chromatographic separation was performed using a DB-SELECT 624UI (Agilent Technologies) column (30 m, 0.32 mm, 1.8 μm stationary phase). The CH_3OH concentration was determined by the average of four successive injections and normalized by total copper content.

Results and discussion

A series of materials with loading ranging from 0.6 to 1.8 wt% Cu was prepared by specific adsorption (SA) with the complex **1** in acetonitrile, where the excess of non-adsorbed precursor was removed by washing with diethyl ether. A second series of copper supported materials was prepared by incipient wetness impregnation (IWI) of **1** in water, achieving copper loadings of 0.3 to 3.2 wt%. Both sets of materials were activated under flow of dry synthetic air at 500 °C to remove the organic moieties and to form the bare Cu-oxo surface species. The materials were stored under inert conditions prior to characterisation.

 This journal is © The Royal Society of Chemistry 2021

Open Access Article. Published on 08 July 2021. Downloaded on 5/21/2026 12:12:38 PM.
This article is licensed under a Creative Commons Attribution 3.0 Unported Licence.

The IWI samples with the lowest and highest Cu loadings (0.3 and 3.2 wt%, respectively) and the SA samples were analysed by powder XRD (pXRD) after activation to confirm the retention of the bulk structure of the transitional γ-Al_2O_3 and to probe the eventual formation of large crystalline CuO particles. For all of the prepared materials, only reflections corresponding to γ-Al_2O_3 were identified, indicating the absence of phase transitions of the support and the absence of large CuO crystallites (Fig. S1 and S2†).

DRIFT analysis of the samples confirmed the complete removal of organic ligands after calcination under synthetic air (Fig. 1a and S2†). For all materials, the presence of –OH moieties on the surface results from the re-hydration of the material by the water released during the thermolysis of the precursor. Only for IWI samples a decrease and shift of the bands located at 3769 cm^{-1}, assigned to terminal μ_1-OH groups on the alumina surface, was observed with increasing copper loading. This observation is consistent with the increasing amount of Cu present on the oxide surface, either by using these hydroxyl groups as anchoring site explaining the decrease of the band, or by interaction inducing a shift of their vibrational frequency (Fig. 1a). In contrast, this band is not affected by the copper loading in the case of the SA samples and all the samples prepared show similar spectral features (Fig. 1c). The difference observed likely originates from a better dispersion of the Cu sites using the specific adsorption method (*vide infra*). Indeed, the maximal Cu loading obtained using the SA approach (1.8 wt% Cu) corresponds to the intermediate loading obtained for the IWI samples (1.6 wt% Cu), allowing the recovery of a greater density of surface hydroxyl at the surface.

To determine copper speciation, the materials were characterized by diffuse reflectance UV-vis spectroscopy (DRUV-vis). Two maxima could be observed in the range measured, at 235 nm and 750 nm, corresponding respectively to the ligand to metal charge transfer (LMCT) of $[Cu^{2+}–O^{-}]$ and the d–d transition of Cu^{2+} in a distorted octahedral geometry.[19] The spectra were normalized to the peak maximum of the LMCT for clarity (insert Fig. 1b–d), allowing the identification of a shoulder at higher wavelength for $Cu_{IWI\text{-}3.2}$, assigned to the $[O^{-}–Cu^{2+}–O^{-}]$ LMCT and indicative of the formation of CuO clusters (Fig. 1b). For the SA sample, this shoulder is absent even for the highest loading of 1.8 wt% Cu (Fig. 1d), similarly to the observation for the intermediate loading obtained by IWI (1.6 wt% Cu). This difference in spectral feature further supports the more homogeneous dispersion of the Cu centres using the SA approach, allowing to avoid the formation of larger CuO clusters.

In addition, temperature programmed reduction (TPR) was performed on the IWI samples to confirm the presence of larger CuO clusters for the highest copper loading (3.2 wt%). The presence of a reduction event at 230 °C could be observed for the highest loaded material ($Cu_{IWI\text{-}3.2}$) and is absent for the materials with lower copper loading (Fig. S3†). This reduction peak is ascribed in the literature to the presence of amorphous copper oxide,[20] consistent with the

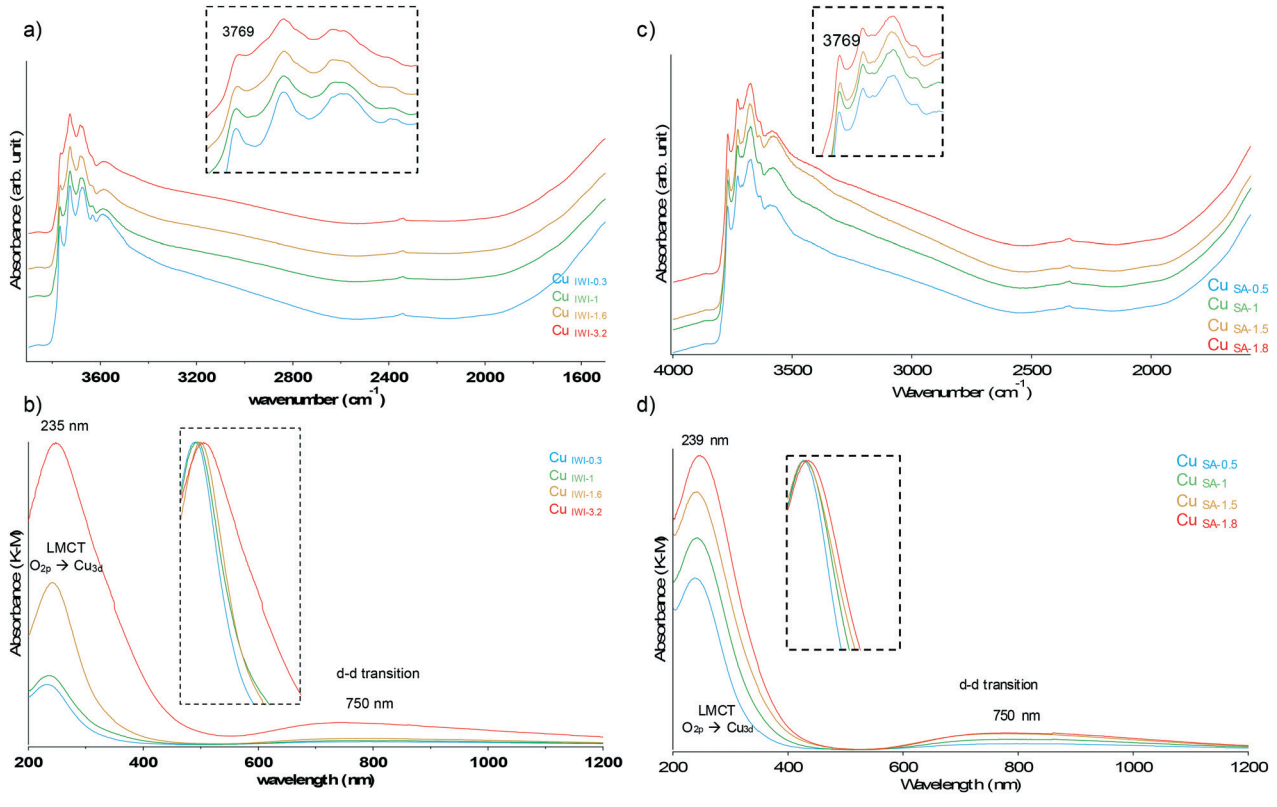

Fig. 1 a–c) DRIFT b–d) DRUV-vis spectra of the IWI (a and b) and SA (c and d) samples after activation at 500 °C under synthetic air.

Open Access Article. Published on 08 July 2021. Downloaded on 5/21/2026 12:12:38 PM.
This article is licensed under a Creative Commons Attribution 3.0 Unported Licence.

absence of diffraction peaks corresponding to CuO by pXRD (Fig. S1†). To investigate the oxidation state and local arrangement of the copper species in the IWI material, continuous wave electron paramagnetic resonance (CW-EPR) and Cu K-edge X-ray absorption near edge spectroscopy (XANES) analysis of the oxygen-activated samples were performed. The XANES spectra are identical for the copper series (Fig. S4†), with the presence of a pre-edge feature at 8978.4 eV, corresponding to the dipole-forbidden quadrupole-allowed 1s → 3d transition for Cu^{2+} species. The low energy of the pre-edge feature indicates a weaker ligand field and low coordination at the copper centre.[21] EPR analysis (Fig. S5†) indicates the presence of copper in an axial environment with a $d_{x^2-y^2}$ ground state ($g_{||} > g_{\perp} > g_e$). The presence of resolved 4 hyperfine lines in the parallel component, arising from the coupling of the unpaired electron with the nuclear spin of Cu^{2+} ($I = 3/2$), is additional evidence for the high dispersion of the copper centres. The broadening observed is indicative of the wide geometrical distribution of Cu^{2+} sites and their magnetic interactions inherent to their proximity. The reactivity of these two sets of materials was then evaluated by contacting the activated material in a closed vessel with 6 bar of methane at 200 °C for 30 min, followed by extraction of the surface intermediates with water at 120 °C. The reactivity is reported in Fig. 2 (Table S1†), in methanol yield normalized by mass of material respectively by mol of Cu.

In all cases except one ($Cu_{SA\text{-}1.8}$), methanol yield (per gram of material) increased with increasing copper loading, while the fraction of active copper, reflected in the methanol yield per mol Cu, decreased with increasing copper loading. For these materials, the methanol yield approaches a maximum value (15 μmol of CH_3OH per g), indicating the formation of a maximum amount of reactive copper sites at high metal coverage (1.3 Cu nm^{-2}). In contrast, reactivity values for $Cu_{SA\text{-}1.8}$ lie above the trends observed for the other samples, yielding 21 μmol of CH_3-OH per g of material (0.075 mol CH_3OH mol^{-1} Cu).

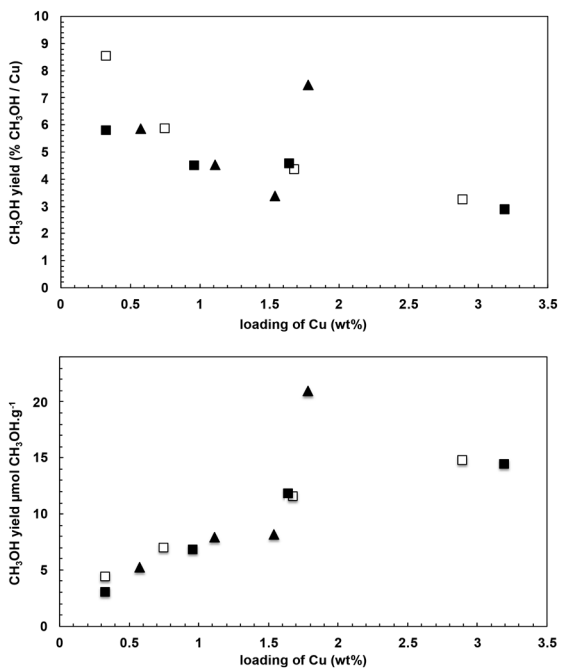

Fig. 2 Reactivity of the IWI samples (■ set 1, □ set 2) and SA samples (▲) as a function of the methanol yield in mol% CH_3OH $mol\%^{-1}$ Cu (top) and μmol g^{-1} (bottom).

To better understand the reactivity observed, the reacted samples were isolated under an inert atmosphere after reaction with methane and analysed by DRIFTS. For all materials, bands at 2951 and 2866 cm^{-1}, previously assigned to methoxy species, and two broad bands at 1615 cm^{-1} and 1589 cm^{-1}, assigned to water and formate species respectively, were observed (Fig. S6 and S7†).

The absence of CO and CO_2 adsorbed on the Cu(I) centres formed and Al sites present at the surface is consistent with the selective formation of methoxy and formate from CH_4 under the studied conditions. Previous work using Al_2O_3 support and Cu(II) aluminate molecular precursor, has shown that the active sites are monomeric Cu^{2+} species, possessing a unique EPR signature.[16] Indeed, EPR spectroscopy is the method of choice providing further information on the configuration and nature of the paramagnetic species, such as Cu^{2+} possessing one unpaired electron (d^9) to be probed. To investigate whether similar reactive centres are generated using IWI and SA as synthesis methods, *in situ* reaction with CH_4 monitored by EPR spectroscopy was performed for all materials (Fig. 3a and S8 and S9†). A decrease of the EPR signal after reaction is observed in all cases and reflects the reduction of isolated monomeric Cu(II) species to EPR silent Cu(I) reacted sites.

Plotting the difference spectra before and after reaction reveals the EPR signature of a single Cu(II) species (site I), corresponding to one of the reactive centres involved in the selective oxidation of methane to methanol (Fig. 3b and S10†). Such sites are identified in all the materials, independently of the preparation method and Cu loading. Similar reactive monomeric Cu(II) centres supported on Al_2O_3 have been previously reported, when employing a molecular approach to generate well-dispersed centre.[16] Low temperature EPR of the material containing the higher portion of dispersed Cu ($Cu_{IWI\text{-}0.3}$) before and after reaction with CH_4 was recorded (Fig. S11†) to extract the parameter of the reactive Cu(II) centre and compare with previously reported Cu(II) monomeric sites. The difference spectra, which correspond to the reactive centre, can be simulated with a nearly axial Cu(II) species with ***g***-tensor parameter g = [2.0625 2.0787 2.3923], and hyperfine coupling A_{Cu} (MHz) = [30 38 400] (Fig. S3c†). Residual features are not fully simulated by the parameters employed, which can be attributed to the broad and heterogeneous distribution of Cu(II) sites on the surface inherent to the preparation method employed. The parameters obtained are associated with reactive tri-coordinated $[(Al_2O)Cu^{II}O(OH)]^-$ sites and corresponds to the one previously reported for Cu(II) monomer on Al_2O_3. Two of these monomers react with CH_4

 This journal is © The Royal Society of Chemistry 2021

Open Access Article. Published on 08 July 2021. Downloaded on 5/21/2026 12:12:38 PM.
This article is licensed under a Creative Commons Attribution 3.0 Unported Licence.

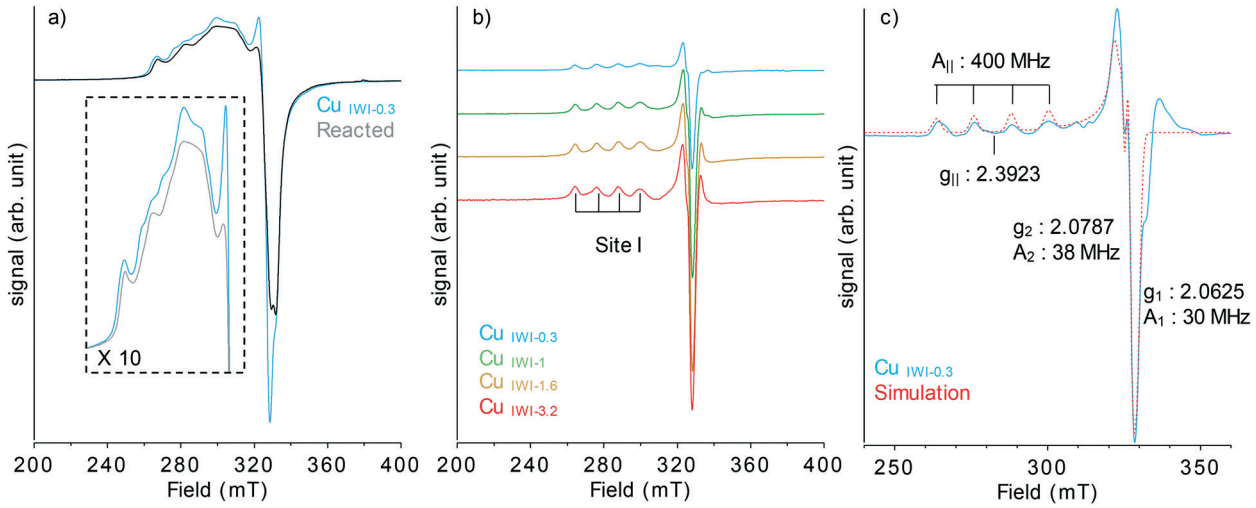

Fig. 3 a) X-band EPR *in situ* reaction of $Cu_{IWI\text{-}0.3}$ with 6 bar of CH_4 at 200 °C for 30 min. The spectra are recorded at 25 °C before and after reaction. b) Resulting difference spectra for the IWI series showing the same spectral signature of the monomeric Cu(II) active site in all samples. c) X-band EPR difference spectrum (−170 °C) for $Cu_{IWI\text{-}0.3}$ before-after reaction (plain) and the resulting simulation (dashed).

by reduction from Cu(II) to Cu(I) centres leading to the formation of CH_3OH according to Scheme 1.

The Al_2O_3 allows for the stabilization and the dispersion of reactive monomeric Cu(II) sites, independently of the method employed for their preparation.

The amount of reduced copper species, determined by calculating the difference between the double integral before and after reaction, was plotted against the methanol yield (Fig. S12†). In all cases, the amount of reduced copper is equal to or more than twice the amount of methanol normalized by copper, consistent with a two-electron methane oxidation process mitigated by two copper ions (Cu^{2+}/Cu^{+}).[22] These results confirm the involvement of two monomeric Cu(II) sites for the partial oxidation of CH_4 to CH_3OH, where the deviation from the theoretical line ($y = \frac{1}{2}x$, corresponding to the maximal CH_3OH yield involving the reduction of 2 Cu(II) → Cu(I) centres) is indicative of the formation of overoxidized by-products, as seen by IR with the formation of formate intermediates surface species. On the basis of this study, the possible contribution of other active Cu(II) centres to the observed reactivity cannot be excluded, as for example the participation of small CuO clusters, not probed by EPR spectroscopy.

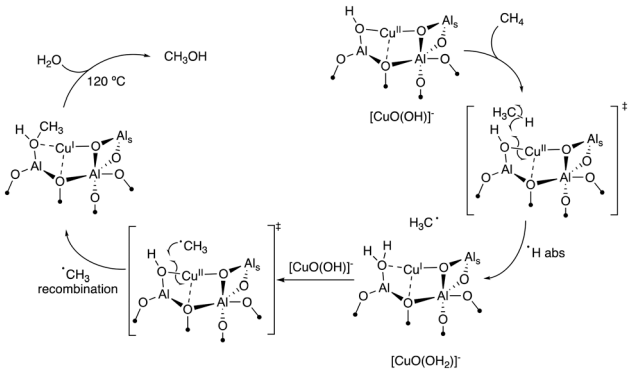

Scheme 1 Possible reaction mechanism for the formation of one CH_3OH molecule by oxidation on two $Cu(O)(OH)^-$ monomers.

Conclusion

We have demonstrated that employing simple preparation methods, namely incipient wetness impregnation and specific adsorption on a commonly used oxidic support like alumina, allows the generation of a reactive material for the selective oxidation of methane to methanol using the stepwise protocol. The previously identified monomeric active site, $[(Al_2O)Cu^{II}O(OH)]^-$, was generated and identified on all the materials independently of the copper loading. In addition to the well-defined monomeric sites, the presence of Cu-oxo oligomeric centres at higher loading cannot be excluded to explain the enhancement of the methanol yield at these loadings. This illustrates the potential of the described straightforward synthetic procedures for the generation and identification of reactive Cu(II) sites on non-zeolitic materials. This methodology, in combination with available characterization techniques, is applicable to a wide range of oxide supports, allowing both the reactivity of the material to be assessed and the active sites to be assigned. This approach could serve as a guideline for the exploration of an extended series of oxide supports and help the design of materials with higher methanol productivity.

Conflicts of interest

There are no conflicts to declare.

Acknowledgements

J. M. thank Shell Global Solutions International B.V. for financial support. We acknowledge Elettra Sincrotrone Trieste

for providing access to its synchrotron radiation facilities and we thank Giuliana Aquilanti and Luca Olivi for measuring the *ex situ* samples (XAFS beamline, proposal 20195503). J. M. would like to acknowledge L. Völker for her help with the XRD data.

Notes and references

1 J. P. Lange, K. P. De Jong, J. Ansorge and P. J. A. Tijm, *Stud. Surf. Sci. Catal.*, 1997, **107**, 81–86.
2 M. Ahlquist, R. J. Nielsen, R. A. Periana and W. A. Goddard, *J. Am. Chem. Soc.*, 2009, **131**, 17110–17115.
3 M. Ravi, M. Ranocchiari and J. A. van Bokhoven, *Angew. Chem., Int. Ed.*, 2017, **56**, 16464–16483.
4 A. A. Latimer, A. Kakekhani, A. R. Kulkarni and J. K. Nørskov, *ACS Catal.*, 2018, **8**, 6894–6907.
5 R. A. Periana, D. J. Taube, S. Gamble, H. Taube, T. Satoh and H. Fujii, *Science*, 1998, **280**, 560–564.
6 N. S. Ovanesyan, V. I. Sobolev, K. A. Dubkov, G. I. Panov and A. A. Shteinman, *The nature of the active oxidant in biomimetic oxidation of methane over Fe-ZSM-5 zeolite*, 1996, vol. 45.
7 M. H. Groothaert, P. J. Smeets, B. F. Sels, P. A. Jacobs and R. A. Schoonheydt, *J. Am. Chem. Soc.*, 2005, **127**, 1394–1395.
8 S. Sirajuddin and A. C. Rosenzweig, *Biochemistry*, 2015, **54**, 2283–2294.
9 D. K. Pappas, A. Martini, M. Dyballa, K. Kvande, S. Teketel, K. A. Lomachenko, R. Baran, P. Glatzel, B. Arstad, G. Berlier, C. Lamberti, S. Bordiga, U. Olsbye, S. Svelle, P. Beato and E. Borfecchia, *J. Am. Chem. Soc.*, 2018, **140**, 15270–15278.
10 A. J. Knorpp, A. B. Pinar, M. A. Newton, V. L. Sushkevich and J. A. van Bokhoven, *ChemCatChem*, 2018, **10**, 5593–5596.
11 V. L. Sushkevich and J. A. Van Bokhoven, *ACS Catal.*, 2019, **9**, 6293–6304.
12 B. E. R. Snyder, M. L. Bols, R. A. Schoonheydt, B. F. Sels and E. I. Solomon, *Chem. Rev.*, 2018, **118**, 2718–2768.
13 H. V. Le, S. Parishan, A. Sagaltchik, H. Ahi, A. Trunschke, R. Schomäcker and A. Thomas, *Chem. – Eur. J.*, 2018, **24**, 12592–12599.
14 S. E. Bozbag, P. Sot, M. Nachtegaal, M. Ranocchiari, J. A. Van Bokhoven and C. Mesters, *ACS Catal.*, 2018, **8**, 5721–5731.
15 J. Meyet, K. Searles, M. A. Newton, M. Wörle, A. P. van Bavel, A. D. Horton, J. A. van Bokhoven and C. Copéret, *Angew. Chem., Int. Ed.*, 2019, **58**, 9841–9845.
16 J. Meyet, A. Ashuiev, G. Noh, M. Newton, D. Klose, K. Searles, A. van Bavel, A. Horton, G. Jeschke, J. A. van Bokhoven and C. Copéret, *Angew. Chem., Int. Ed.*, 2021, **60**, 16200.
17 T. Margossian, K. Larmier, F. Allouche, K. W. Chan and C. Copéret, *Helv. Chim. Acta*, 2019, **102**, e1800227.
18 A. Di Cicco, G. Aquilanti, M. Minicucci, E. Principi, N. Novello, A. Cognigni and L. Olivi, *J. Phys.: Conf. Ser.*, 2009, **190**, 012043.
19 J. J. Bravo-Suárez, B. Subramaniam and R. V. Chaudhari, *J. Phys. Chem. C*, 2012, **116**, 18207–18221.
20 W. P. Dow, Y. P. Wang and T. J. Huang, *Appl. Catal., A*, 2000, **190**, 25–34.
21 K. I. Shimizu, H. Maeshima, H. Yoshida, A. Satsuma and T. Hattori, *Phys. Chem. Chem. Phys.*, 2001, **3**, 862–866.
22 M. A. Newton, A. J. Knorpp, A. B. Pinar, V. L. Sushkevich, D. Palagin and J. A. Van Bokhoven, *J. Am. Chem. Soc.*, 2018, **140**, 10090–10093.

Open Access Article. Published on 08 July 2021. Downloaded on 5/21/2026 12:12:38 PM.
This article is licensed under a Creative Commons Attribution 3.0 Unported Licence.

This journal is © The Royal Society of Chemistry 2021